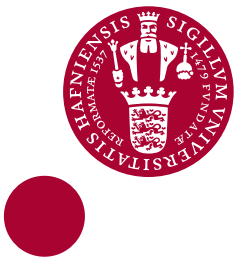

Nanomechanical single-photon routing

Papon, Camille; Zhou, Xiaoyan; Nielsen, Henri Thyrrestrup; Liu, Zhe; Stobbe, Søren; Schott, Rüdiger; Wieck, Andreas D.; Ludwig, Arne; Lodahl, Peter; Midolo, Leonardo

Published in:
Optica

DOI:
10.1364/OPTICA.6.000524

Publication date:
2019

Document version
Publisher's PDF, also known as Version of record

Research Article Vol. 6, No. 4 / April 2019 / Optica 524

Nanomechanical single-photon routing

Camille Papon,[1,†] Xiaoyan Zhou,[1,†] Henri Thyrrestrup,[1] Zhe Liu,[1] Søren Stobbe,[2,3] Rüdiger Schott,[4] Andreas D. Wieck,[4] Arne Ludwig,[4] Peter Lodahl,[1] and Leonardo Midolo[1,*]

[1]Center for Hybrid Quantum Networks (Hy-Q), Niels Bohr Institute, University of Copenhagen, Blegdamsvej 17, 2100-DK Copenhagen, Denmark
[2]Niels Bohr Institute, University of Copenhagen, Blegdamsvej 17, 2100-DK Copenhagen, Denmark
[3]Currently with the Department of Photonics Engineering, DTU Fotonik, Technical University of Denmark, Building 343, 2800 Kongens Lyngby, Denmark
[4]Lehrstuhl für Angewandte Festkörperphysik, Ruhr-Universität Bochum, Universitätsstrasse 150, D-44780 Bochum, Germany
*Corresponding author: midolo@nbi.ku.dk

Received 31 January 2019; revised 18 March 2019; accepted 23 March 2019 (Doc. ID 359234); published 19 April 2019

The active routing of photons using rapid reconfigurable integrated circuits is a key functionality for quantum-information processing. Typical waveguide-based optical switches rely on the modulation of the refractive index, producing a modest variation of the phase of the optical fields. Mechanical motion of nanophotonic structures, on the contrary, can be tailored to produce a much larger effect, without introducing loss or emitter decoherence and operating at a speed matching the quantum memory storage time of the on-chip quantum emitter. Here we demonstrate a compact and low-loss nano-opto-electromechanical single-photon router, based on two coupled waveguides whose distance is adjusted on demand by an external voltage. We show controllable two-port routing of single photons emitted from quantum dots embedded in the same chip. We report a maximum splitting ratio >23 dB, insertion loss of 0.67 dB, and sub-microsecond response time. The device is an essential building block for constructing advanced quantum photonic architectures on-chip, towards, e.g., coherent multi-photon sources, deterministic photon–photon quantum gates, quantum-repeater nodes, or scalable quantum networks.

https://doi.org/10.1364/OPTICA.6.000524

1. INTRODUCTION

Photonic quantum technologies offer unprecedented opportunities to implement quantum optics experiments directly on a chip, thereby replacing large-scale optical setups with integrated devices interfacing high-efficiency single-photon emitters, waveguide circuitry, and detectors [1]. Scaling up to multi-qubit systems is the key challenge, and to this end modern device nanofabrication is a major asset. While significant progress has been made in the fabrication of advanced quantum optical circuits for processing single photons [2–4] towards, e.g., quantum computing [5], it appears very demanding to scale up quantum processors based on linear optics alone [6]. It is therefore highly desirable to develop additional photonic quantum resources in order to break new grounds.

The development of a deterministic and coherent interface between a single photon and a single emitter, as recently demonstrated with atoms [7,8], defect centers [9], and quantum dots [10], leads to novel opportunities for quantum photonics. It enables constructing multi-photon sources [11], photon–photon quantum gates [12], nonlinear operations at the single-photon level [13], and the generation of multi-photon entangled cluster states [14]. Application areas include device-independent quantum key distribution [15], all-photonic quantum repeaters [16,17], photonic quantum computing [18], and connecting distant and heterogeneous quantum nodes via a photonic network [19]. As a quantitative benchmark, it has been estimated that photon coupling efficiencies beyond 90% and local processing speeds faster than 100 ns are required in order to develop advantageous all-photonic quantum-repeater protocols [20], which is challenging yet feasible with, e.g., quantum dots embedded in nanophotonic waveguides [21]. It is here essential to be able to reconfigure the circuit and route photonic qubits between different quantum nodes [see Fig. 1(a)] with very low loss and at a speed that is compatible with the emitter qubit coherence time, which for efficient solid-state emitters such as quantum dots and defect centers is typically in the range of microseconds to milliseconds [22,23]. Unlike in classical communications, where amplification is possible, optical losses pose a fundamental bottleneck when routing single photons, due to the impossibility of cloning a quantum state. For this reason, such low-loss, tunable, and fast photonic circuitry has not yet been implemented on devices containing active photon emitters and spins, and existing tuning mechanisms based on thermal heating and the electro-optic effect do not meet these demands: while the thermo optic effect is slow and not compatible with cryogenic operation, the electro-optic effect is material-dependent and typically results in a large device footprint with constraints for scaling and efficiency. Consequently, a fundamentally different approach is required.

In this work, we merge the two research disciplines of deterministic photon-emitter interfaces and nano-opto-electromechanics in order to bridge that gap. Electrically induced mechanical deformation of the waveguide circuit constitutes a novel and elegant

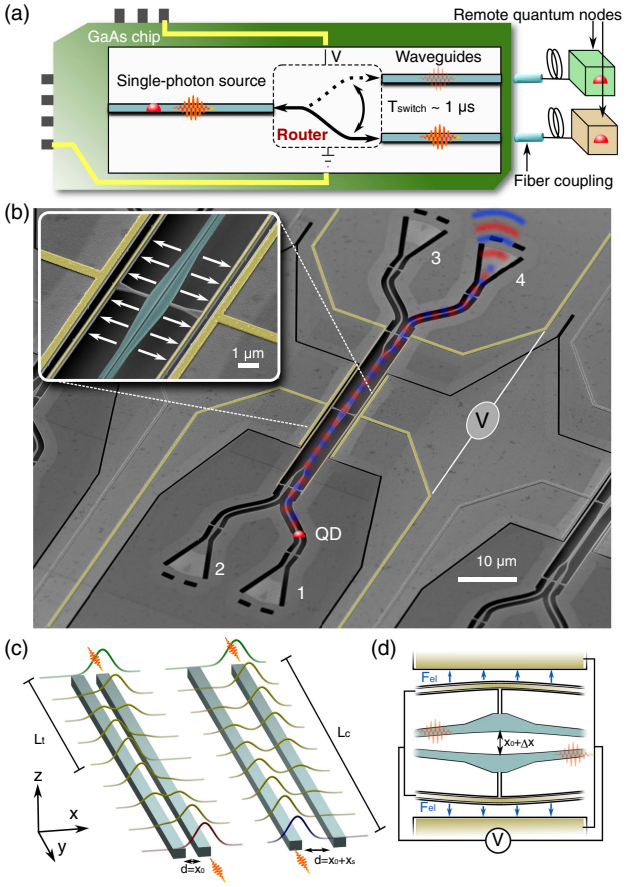

Fig. 1. Operational principle of nanomechanical single-photon routing. (a) On-chip quantum node based on a quantum emitter and a fast single-photon router. (b) False-color scanning electron micrograph of the single-photon router. The electrodes are highlighted in yellow. The numbers indicate the in- and out-coupling ports of the device, and the red spot marks the approximate position of the quantum dot used for the experiment. An artistic representation of the propagating optical electric field is overlaid on the figure. The inset shows a zoom-in of the central section of the device where the waveguides have been highlighted in blue and white arrows indicate the mechanical motion. (c) Operation principle of a tunable directional coupler made of suspended dielectric waveguides, which is the basic element for mechanical routing. (d) Schematic view of the electromechanical actuator and induced deformation (not to scale). When a bias voltage V is applied to the electrodes, a force F_{el} pulls the waveguides apart, enabling the routing operation.

approach to photon routing, which is independent of intrinsic material properties and therefore can be implemented for many material systems, wavelengths, and temperatures [24], including for active photonic chips containing quantum emitters [25–27]. At the nanoscale, the opto-electromechanical interaction is much stronger than refractive-index tuning effects. Therefore, the device footprint, switching time, and insertion loss are significantly reduced, meaning that circuit complexity can be scaled up. We present a compact ($\sim 5 \times 30\ \mu m^2$) directional coupler with variable coupling strength, adjustable by means of integrated electrostatic actuators. Unlike previous works with mechanically tunable directional couplers [27], where out-of-plane actuation is used to switch off the coupling entirely, here we use in-plane motion that does not break the device symmetry, thereby enabling a continuously reconfigurable splitting ratio at any wavelength and, more importantly, a scalable architecture. We demonstrate full and reversible switching of single photons at cryogenic temperatures with an applied voltage of 10 V, corresponding to a <70 nm mechanical motion, a maximum splitting ratio of (23.4 ± 1.7) dB or $(99.5/0.5 \pm 0.2)\%$, insertion loss of 0.67 dB, and response time below 1 μs, limited by the fundamental mechanical resonance at 1.36 MHz. The device length ($L = 26\ \mu m$) and the measured switching voltage result in a low $V_\pi L = 0.026$ Vcm figure of merit, which is an order of magnitude smaller than recent state-of-the-art electro-optic phase shifters [28]. As a quantitative prospect of the technology, we estimate that a single-qubit unitary gate composed of a controllable beam splitter and a phase shifter could be built with a footprint smaller than 30 μm^2 and with a response time of 100–200 ns. With such an approach, fully integrated photonic quantum processing may be within reach.

2. NANOMECHANICAL CONTROL OF DIRECTIONAL COUPLERS

The integrated photon router has been fabricated in thin GaAs membranes with embedded InAs quantum dots; cf. the scanning electron micrograph (SEM) of Fig. 1(b). It consists of suspended dielectric waveguides connected to capacitive nanomechanical actuators, whose role is to convert a voltage signal into the mechanical motion required for optical switching. The principle of operation is that of a gap-variable directional coupler with an adjustable coupling strength $g \propto \exp(-\kappa d)$, where κ is the spatial decay of the fundamental transverse electric mode supported by each individual waveguide and d is the waveguide separation. Figure 1(c) shows schematically the propagation of light in such a device when initially illuminated through one port only. If the waveguides are identical (phase matching condition), the optical power is fully transferred to the other waveguide after a transfer length $L_t(d) = \pi/(2g(d))$. At the end of the coupling section (length L_c) the splitting ratio is

$$\mathrm{SR} = \tan^2\left(\frac{\pi L_c}{2L_t(d)}\right). \quad (1)$$

To tune the splitting ratio, d can be changed using an external force to induce a $\pi/2$ change in the argument of Eq. (1). The exponential dependence of L_t on d implies that it is advantageous to work at small separations (nano-slots) in order to increase the sensitivity of the splitting ratio to small deformations and to reduce the device footprint [24]. In this work, the highest sensitivity $L_c \frac{dg}{dx}$ is roughly $\simeq 20$ mrad/nm, sufficiently low to neglect thermo-mechanical or electrical noise. Full switching is only possible if light transfers at least once from one waveguide to the next, i.e., $L_c > L_t$, suggesting a device scaling law, which is directly proportional to the transfer length at rest, or $\propto \exp(\kappa x_0)$, where x_0 is the initial gap between the waveguides. Reducing the gap to a few tens of nanometers, which is realistic with current fabrication technology, would imply that a coupling length below 5 μm could be achieved, showing the huge integration potential of nanomechanical switches. For further information about the theory of gap-variable directional couplers, see Section 2 of Supplement 1.

The mechanical deformation is obtained by capacitive actuation, as shown schematically in Fig. 1(d) and visible in the SEM image of Fig. 1(b). Each waveguide is connected via thin tethers to a pair of electrodes forming gap-variable capacitors whose distance at rest is 300 nm in the current device. When a bias voltage is applied across the electrodes, they bend and increase the

waveguide separation by Δx. This geometry allows us to double the displacement of a single actuator by electrically wiring both sides of the device in parallel. See Section 3 of Supplement 1 for details on the device design.

3. CHARACTERIZATION OF THE TUNABLE BEAM SPLITTER

The device is characterized at cryogenic temperature ($T = 10$ K) in a Helium flow cryostat. Room-temperature results are presented and discussed in Section 4 of Supplement 1. A supercontinuum source is focused into either port 1 or port 2 [see Fig. 1(b) for port numbering], and the output is collected at ports 3 and 4 and analyzed with a spectrometer. The splitting ratio between port 3 and port 4 as a function of wavelength and applied bias can be determined by a total of four measurements using

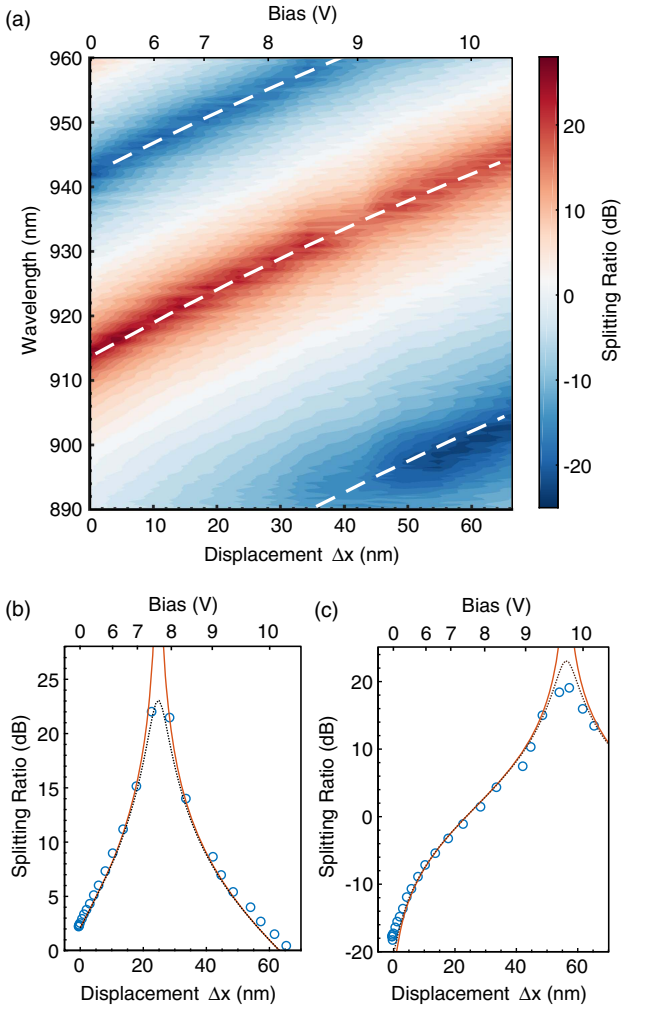

Fig. 2. Tunable splitting ratio and wavelength dependence. (a) Map of the measured splitting ratio obtained from four independent transmission measurements as a function of the total waveguide displacement Δx and wavelength. The dashed lines indicate the theoretical curves for maximum transmission and extinction used for calibrating the displacement as a function of voltage. (b),(c) Measured (blue circles) and simulated (red solid lines) splitting ratio as a function of displacement for two wavelengths of interest. In (b) $\lambda_0 \sim 927$ nm is the wavelength used for switching the QD emission, and in (c) $\lambda_0 \sim 941$ nm is a wavelength where full switching can be performed. The dotted line shows the simulated device in the case of a finite splitting ratio.

$$\mathrm{SR} = \sqrt{\frac{I_{31} \cdot I_{42}}{I_{41} \cdot I_{32}}}, \tag{2}$$

where I_{ji} is the transmitted intensity from the input port i to the output port j. In this way, we compensate for the in-coupling and out-coupling efficiencies of the individual gratings and fiber-couplers (see Section 4 of Supplement 1). Figure 2(a) shows a map of the splitting ratio in decibels, i.e., $10\log_{10}(\mathrm{SR})$. By adjusting the voltage, the splitting ratio can be tuned over a broad wavelength range of 70 nm corresponding to the bandwidth of the out-coupling gratings. To explain the dispersive response accurately, a theoretical model of the SR is developed, which takes into account the spectral dispersion of GaAs at 10 K, and the fact that the separation between the waveguides is not uniform across its length (see Section 4 of Supplement 1). The bending of the waveguides results in an effective coupling factor $g_{\mathrm{eff}}(\lambda, d_{\mathrm{max}})$, where d_{max} denotes the maximum distance between the waveguides. The numerical model provides a set of contour lines, which represent points of equal values of $g_{\mathrm{eff}}L_c$ (i.e., identical SR). The white dashed lines in Fig. 2(a) indicate these contours for maximum and minimum SR. We use the central line (starting at $\lambda_0 = 914$ nm at 0 V) to map the voltage to the theoretical displacement. The result provides the bottom linear axis for the figure, while the top nonlinear axis indicates the corresponding voltage used in the experiment. The theoretical model explains the experimental data very well, as exemplified for the two cross-section cuts of the data presented in Figs. 2(b) and 2(c), at $\lambda_0 = 927$ nm and $\lambda_0 = 941$ nm, respectively. These wavelengths are chosen as they correspond to two QD emission lines in the device, whose data is shown in Fig. 3 and Fig. S6(a) of Supplement 1. The solid line indicates the numerical model with perfect phase matching and thus an infinite splitting ratio. The finite experimental splitting ratio of up to 23 dB is explained by introducing a small mismatch in the propagation constants of the two waveguides of approximately 7%, which is attributed to a slight non-adiabatic transition to the coupling region.

4. SINGLE-PHOTON ROUTING

The data of Fig. 3 show the ability to perform high-extinction routing of single photons emitted from single quantum dots (QDs) in the device. Figure 3(a) shows an emission spectrum when optically exciting multiple QD emission lines that can be spectrally selected. By displacing the waveguides with voltage, the emitted photons from each QD are distributed to the two output ports as indicated in the inset. Unlike thermo-optic methods [29], the mechanical motion is decoupled from the QD, which is confirmed by the absence of detuning of the excitonic emission. Consequently, the device enables disturbance-free routing of single photons from the embedded QDs.

We focus on the QD located at a wavelength of 927.26 nm. The integrated counts as a function of displacement are plotted in Fig. 3(b) and normalized according to the coupling efficiency (see Section 4 of Supplement 1 for details). The applied voltage is stepped over the 0–10.2 V range multiple times to test the reproducibility of the switching curve, resulting in the small deviations of the integrated counts indicated by the error bars. A maximum extinction ratio of (23.4 ± 1.7) dB is measured at a displacement of 24 nm (i.e., at a bias voltage of 7 V) corresponding to a splitting ratio of $(99.5/0.5 \pm 0.2)\%$. The solid lines show

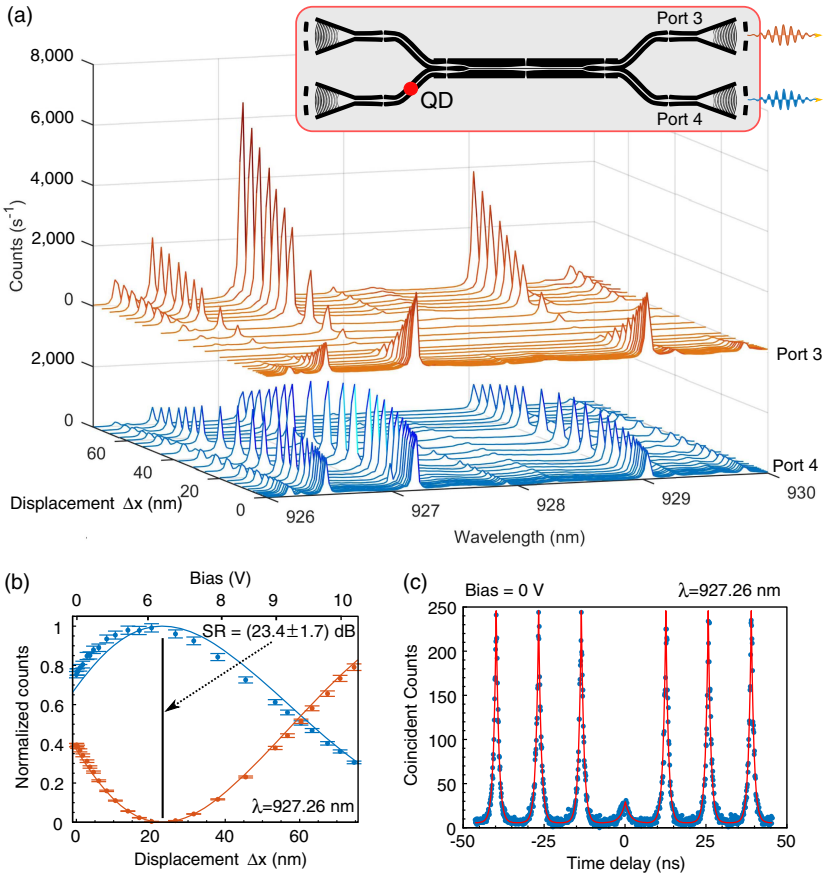

Fig. 3. Routing single photons from quantum dots. (a) Spectra collected from port 3 (red lines above) and 4 (blue lines below) from a quantum dot positioned in the input arm as shown schematically in the inset. Several transitions are modulated in intensity by the waveguide motion, displaying a pronounced anti-correlation between the two ports. (b) Integrated and normalized intensity at ports 3 and 4 for a single exciton line located at $\lambda = 927.26$ nm. The error bar indicates the standard deviation due to multiple voltage scans over the same transition. The solid lines represent the numerical simulation. (c) Second-order auto-correlation measurement of the signal collected from port 3 with no bias voltage applied, showing anti-bunching at zero delay and confirming single-photon emission from the QD.

the theoretical model used to calibrate the displacement in the transmission measurements. A small drift in the electromechanical response of the actuator, probably related to thermal excursions in the time between measurements ($>5h$), is observed when comparing the displacement scales of Figs. 3 and 2. Yet, very good agreement with the model of a loss-less and perfectly balanced router is observed, whereas minor deviations are attributed to a small residual reflectivity from the gratings. These data show that QD emission can be routed on-chip with exceedingly high extinction. Notably, the demonstrated performance is on par with the extinction values previously demonstrated on single Mach–Zehnder interferometers with thermo-optic phase shifters (i.e., in the 20–30 dB range). It could even be further improved by adopting a double-gate approach of cascading a second tunable routing circuit to direct any residual unwanted signal to a third idle output port [30]. Furthermore, the static power consumption obtained by measuring the leakage current across the electrodes is below 50 nW, which is expected for electromechanical actuators. Such low power consumption is crucial to avoid crosstalk in dense switching networks, while high-extinction single-photon routing on the same chip as the emitter is key in order to construct deterministic quantum gates for photons.

To confirm the single-photon nature of the routing, we perform a pulsed Hanbury–Brown and Twiss experiment. A bandpass filter (0.3 nm bandwidth) is used to select only one emission line from the QD spectrum. The experimental setup is shown schematically in Fig. S6(b) of Supplement 1. The measured second-order auto-correlation function, $g^{(2)}(\tau)$, is shown in Fig. 3(c) at a power $P = 0.4P_{\mathrm{sat}}$ ($P_{\mathrm{sat}} = 0.2$ μW is the saturation power of the QD), and the peaks are modeled with exponential functions. The recorded single-photon purity ($g^{(2)}(0) = 0.18 \pm 0.03$) is limited by the density of QDs and the applied above-band excitation scheme, and could readily be improved further [31]. The low insertion loss of the device is confirmed by recording the total photon count rate from the device. No evidence of increased loss from the photon router was observed, since the recorded count rate on the present device was comparable to similar devices without the presence of an active routing section. From these measurements, an insertion loss below 0.67 dB/switch is obtained. Note also that the device comprises engineered gratings for highly efficient (>60%) coupling from the chip to an optical fiber [32]. See Section 4 of Supplement 1 for further details on the analysis of the device efficiency.

The demonstrated performance of the single-photon router directly opens new opportunities for quantum photonics. As a concrete example, a de-multiplexed source of N single photons can be constructed by using a single deterministically coupled emitter combined with low-loss and high-contrast routing. By cascading the nanomechanical routers, a 10-photon source can be achieved, which is significantly beyond current state-of-the-art of $N = 5$

using bulk electro-optical modulators [11]. With the use of QDs at telecom wavelengths [33] and further realistic improvements of the device, the technology could be scaled up to $N > 50$. For comparison, certain quantum algorithms, such as boson sampling, are expected to show quantum advantage for $N = 50$ [34]. Detailed estimates of the achievable multi-photon generation rates are presented in Section 7 of Supplement 1. It should be emphasized that these advantageous resource estimates are performed for the specific case of emitting independent photons, while adding, e.g., the spin quantum memory could lead to even more efficient generation of non-trivial photonic quantum resources.

5. TIME RESPONSE

Micro-electro-mechanical and thermo-optic switches are known for their slow response, i.e., in the kilohertz range. A nanomechanical router, on the other hand, allows pushing this boundary further, entering the megahertz regime. Such fast switching is required in quantum-information protocols exploiting solid-state quantum memories, such as a single spin in a QD [22]. The time response of the nanomechanical single-photon router is determined by the mechanical susceptibility of the actuator, i.e., by its mechanical quality factor Q_m and its fundamental resonant frequency ν_m, which sets an upper limit to the switching rate. Figure 4(a) shows the calculated in-plane mechanical resonant mode. For a perfectly symmetric structure, two fundamental and degenerate in-plane resonances are found numerically, with $\nu_m = 1.36$ MHz. The mechanical quality factor at cryogenic temperatures and in vacuum is mainly determined by the clamping losses, which for suspended bridge geometries at these scales gives $Q_m \sim 10^3$–10^4 [35]. Details on the mechanical spectrum and its measurement are given in Section 6 of Supplement 1.

Ideally, a critically damped (i.e., $Q_{m,c} = 1/2$) resonator can respond to step signals within a time as short as $\nu_m^{-1} \simeq 735$ ns without oscillations. In this mode of operation, it is therefore desirable to increase the damping, which in the experiment can be done by operating the device at atmospheric pressure. Critical damping at cryogenic conditions can be achieved, e.g., by introducing an inert buffer gas into the cryostat. A continuous-wave laser is directed to one input port of the device while a step voltage drives the actuator [see Fig. 4(a)]. The applied bias of 4 V is sufficiently low to ensure that the laser intensity at the output is only weakly modulated and therefore proportional to the waveguide displacement, allowing us to probe the mechanical motion optically. The intensity-modulated laser output is collected into a fiber connected to a fast avalanche photodiode, whose electrical signal is measured on an oscilloscope. Ring-down measurements have been performed with a variable ramp-down time Δt to investigate the time scales involved in the mechanical response. The time traces of the photodiode signal (and applied bias) are shown in Figs. 4(b) and 4(c), for $\Delta t = 100$ ns and $\Delta t = 1$ µs, respectively.

Figure 4(b) illustrates the case in which the force on the actuator is suddenly released over a time Δt much shorter than the natural period of the device, i.e., when $\Delta t < \nu_m^{-1}$. Therefore, the input signal excites the fundamental mechanical resonance of the waveguides, and the device responds with damped oscillations. The inset of Fig. 4(b) shows the Fourier transform of the damped signal (highlighted in red), revealing a single mechanical resonance at $\nu_m = 1.35$ MHz (in accordance with numerical calculations) and with $Q_{m,\mathrm{air}} = 11.5$. This mode of operation is useful

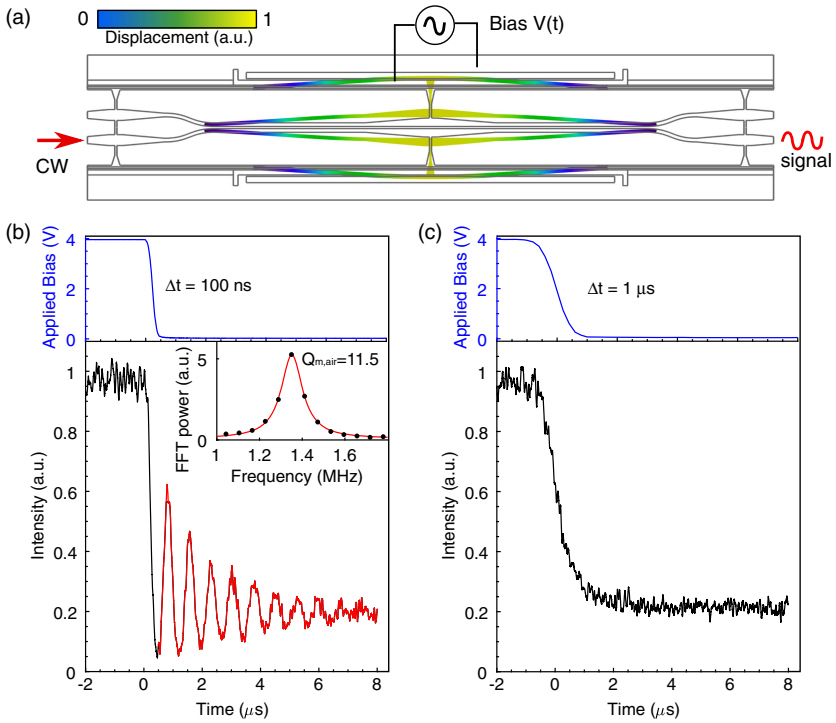

Fig. 4. Time-domain response of the single-photon router. (a) Finite element simulation of the fundamental in-plane mechanical mode overlaid on the un-deformed device geometry. The time-domain response is investigated by driving the actuator with a time-variable voltage $V(t)$ and probing its motion with a continuous-wave (CW) laser. (b) Measured ring-down response of the system with air damping. A step voltage (top graph) is applied and released over a time $\Delta t = 100$ ns, inducing damped oscillations in the response (bottom graph). The inset shows the fast Fourier transform (FFT) power of the ring-down signal. (c) Same as (b) but with a transition time $\Delta t = 1$ µs, showing that the router can be reconfigured within that time interval.

to identify the mechanical resonances of the device but does not correspond to a situation in which the device is rapidly and deterministically reconfigured. Indeed, the time required for the mechanical oscillations to stabilize is approximately $Q_{m,\mathrm{air}}/\nu_m \simeq 8$ μs. For certain applications, resonant driving of the device may be favorable, e.g., in synchronized switching of photons in a de-multiplexing setup aimed at transforming one deterministic single-photon source into multiple sources [21]. In this case, boosting the quality factor Q_m to higher values by, e.g., suppressing clamping losses could be advantageous to achieve ultra-low switching voltages in the millivolt regime. Additional data on resonant driving are presented in Section 6 of Supplement 1.

When $\Delta t > \nu_m^{-1}$ [see Fig. 4(c)], the mechanical response follows the dynamics of the input signal and stabilizes within approximately 1 μs. It is found that the device can be driven without exciting any mechanical resonances of the device; i.e., this is the mode of operation of reconfigurable photon routing that is demonstrated on the microsecond time scale. This would be useful for programming arbitrary sequences of qubit rotations or quickly routing single photons into various channels, as illustrated schematically in Fig. 1(a). We emphasize that the resonant frequency scales with the device length according to $\nu_m \propto L^{-2}$; hence the response time could be significantly reduced to ∼0.1 μs by designing shorter coupling lengths. These time scales of deterministic on-chip single-photon routing offer new opportunities for high-speed quantum communication.

6. CONCLUSION

We have demonstrated an on-chip reconfigurable circuit, which was used for routing single photons emitted from QDs. The router exhibits low insertion loss of 0.67 dB, high extinction ratio >23 dB, and a response time below 1 μs, approaching the coherence time of single spins in QDs. The small footprint and the planar design will allow cascading multiple devices in a single chip, enabling more complex routing schemes. The concept could be readily transferred to other material platforms containing high-quality solid-state emitters, such as vacancy centers in diamond, as well as to other wavelengths. A path towards making even smaller and faster devices is to further reduce the waveguide separation [24]. This could be achieved by, for example, reversing the direction of actuation or fabricating smaller waveguide slots. The seamless integration with QDs makes the presented device an ideal platform for source-integrated reconfigurable quantum photonic circuits. It allows the integration of hybrid systems involving quantum emitters, electrical devices, and mechanical resonators, which have recently drawn much attention for precision sensing [36]. A scalable reconfigurable single-photon router is the cornerstone of protocols for de-multiplexing single-photon sources [37], boson sampling, and linear-optical quantum computing. Furthermore, this device could be combined with mechanically tunable phase shifters [38], in providing a path to programmable nanomechanical unitary gates. Together with deterministic positioning of QDs, efficient out-coupling schemes, and detectors, this approach will enable advanced quantum-information processing applications with single photons beyond the linear-optics quantum computing paradigm that has been inspirational to integrated quantum photonics research.

Funding. Innovationsfonden (Quantum Innovation Center QUBIZ); Villum Fonden; Danmarks Grundforskningsfond (DNRF) (Center for Hybrid Quantum Networks (Hy-Q)); H2020 European Research Council (ERC) (SCALE); Teknologi og Produktion, Det Frie Forskningsråd (FTP, DFF) (4184-00203); Bundesministerium für Bildung und Forschung (BMBF) (16KIS0867, Q.Link.X); Deutsche Forschungsgemeinschaft (DFG) (TRR 160); Styrelsen for Forskning og Innovation (FI) (5072-00016B QUANTECH).

Acknowledgment. We acknowledge Tommaso Pregnolato for assistance in fabrication and Sofie Lindskov Hansen, Ravitej Uppu, and Andrea Fiore for useful discussions.

See Supplement 1 for supporting content.

[†]These authors contributed equally to this work.

REFERENCES

1. J. L. O'Brien, A. Furusawa, and J. Vučković, "Photonic quantum technologies," Nat. Photonics **3**, 687–695 (2009).
2. A. Politi, M. J. Cryan, J. G. Rarity, S. Yu, and J. L. O'Brien, "Silica-on-silicon waveguide quantum circuits," Science **320**, 646–649 (2008).
3. A. Crespi, R. Osellame, R. Ramponi, D. J. Brod, E. F. Galvão, N. Spagnolo, C. Vitelli, E. Maiorino, P. Mataloni, and F. Sciarrino, "Integrated multimode interferometers with arbitrary designs for photonic boson sampling," Nat. Photonics **7**, 545–549 (2013).
4. J. Wang, S. Paesani, Y. Ding, R. Santagati, P. Skrzypczyk, A. Salavrakos, J. Tura, R. Augusiak, L. Mančinska, D. Bacco, D. Bonneau, J. W. Silverstone, Q. Gong, A. Acín, K. Rottwitt, L. K. Oxenløwe, J. L. O'Brien, A. Laing, and M. G. Thompson, "Multidimensional quantum entanglement with large-scale integrated optics," Science **360**, 285–291 (2018).
5. E. Knill, R. Laflamme, and G. J. Milburn, "A scheme for efficient quantum computation with linear optics," Nature **409**, 46–52 (2001).
6. T. Rudolph, "Why I am optimistic about the silicon-photonic route to quantum computing," APL Photon. **2**, 030901 (2017).
7. J. D. Thompson, T. G. Tiecke, N. P. de Leon, J. Feist, A. V. Akimov, M. Gullans, A. S. Zibrov, V. Vuletić, and M. D. Lukin, "Coupling a single trapped atom to a nanoscale optical cavity," Science **340**, 1202–1205 (2013).
8. A. Reiserer and G. Rempe, "Cavity-based quantum networks with single atoms and optical photons," Rev. Mod. Phys. **87**, 1379–1418 (2015).
9. A. Sipahigil, R. E. Evans, D. D. Sukachev, M. J. Burek, J. Borregaard, M. K. Bhaskar, C. T. Nguyen, J. L. Pacheco, H. A. Atikian, C. Meuwly, R. M. Camacho, F. Jelezko, E. Bielejec, H. Park, M. Lončar, and M. D. Lukin, "An integrated diamond nanophotonics platform for quantum-optical networks," Science **354**, 847–850 (2016).
10. P. Lodahl, S. Mahmoodian, and S. Stobbe, "Interfacing single photons and single quantum dots with photonic nanostructures," Rev. Mod. Phys. **87**, 347–400 (2015).
11. H. Wang, Y. He, Y.-H. Li, Z.-E. Su, H.-L. Huang, X. Ding, M.-C. Chen, C. Liu, J. Qin, J.-P. Li, Y.-M. He, C. Schneider, M. Kamp, C.-Z. Peng, S. Höfling, C.-Y. Lu, and J.-W. Pan, "High-efficiency multiphoton boson sampling," Nat. Photonics **11**, 361–365 (2017).
12. L. M. Duan and H. J. Kimble, "Scalable photonic quantum computation through cavity-assisted interactions," Phys. Rev. Lett. **92**, 127902 (2004).
13. D. E. Chang, A. S. Sørensen, E. A. Demler, and M. D. Lukin, "A single-photon transistor using nanoscale surface plasmons," Nat. Phys. **3**, 807–812 (2007).
14. N. H. Lindner and T. Rudolph, "Proposal for pulsed on-demand sources of photonic cluster state strings," Phys. Rev. Lett. **103**, 113602 (2009).
15. A. Máttar, J. Kołodyński, P. Skrzypczyk, D. Cavalcanri, K. Banaszek, and A. Acín, "Device-independent quantum key distribution with single-photon sources," arXiv:1803.07089 (2018).
16. K. Azuma, K. Tamaki, and H.-K. Lo, "All-photonic quantum repeaters," Nat. Commun. **6**, 6787 (2015).
17. D. Buterakos, E. Barnes, and S. E. Economou, "Deterministic generation of all-photonic quantum repeaters from solid-state emitters," Phys. Rev. X **7**, 041023 (2017).

18. H. Pichler, S. Choi, P. Zoller, and M. D. Lukin, "Universal photonic quantum computation via time-delayed feedback," Proc. Natl. Acad. Sci. USA **114**, 11362–11367 (2017).
19. B. Hensen, H. Bernien, A. E. Dréau, A. Reiserer, N. Kalb, M. S. Blok, J. Ruitenberg, R. F. L. Vermeulen, R. N. Schouten, C. Abellán, W. Amaya, V. Pruneri, M. W. Mitchell, M. Markham, D. J. Twitchen, D. Elkouss, S. Wehner, T. H. Taminiau, and R. Hanson, "Loophole-free Bell inequality violation using electron spins separated by 1.3 kilometres," Nature **526**, 682–686 (2015).
20. S. Muralidharan, L. Li, J. Kim, N. Lütkenhaus, M. D. Lukin, and L. Jiang, "Optimal architectures for long distance quantum communication," Sci. Rep. **6**, 20436 (2016).
21. P. Lodahl, "Quantum-dot based photonic quantum networks," Quantum Sci. Technol. **3**, 013001 (2018).
22. R. J. Warburton, "Single spins in self-assembled quantum dots," Nat. Mater. **12**, 483–493 (2013).
23. D. D. Sukachev, A. Sipahigil, C. T. Nguyen, M. K. Bhaskar, R. E. Evans, F. Jelezko, and M. D. Lukin, "Silicon-vacancy spin qubit in diamond: a quantum memory exceeding 10 ms with single-shot state readout," Phys. Rev. Lett. **119**, 223602 (2017).
24. L. Midolo, A. Schliesser, and A. Fiore, "Nano-opto-electro-mechanical systems," Nat. Nanotechnol. **13**, 11–18 (2018).
25. R. Perahia, J. D. Cohen, S. Meenehan, T. P. Mayer Alegre, and O. Painter, "Electrostatically tunable optomechanical "zipper" cavity laser," Appl. Phys. Lett. **97**, 191112 (2010).
26. L. Midolo, F. Pagliano, T. B. Hoang, T. Xia, F. W. M. van Otten, L. H. Li, E. H. Linfield, M. Lermer, S. Höfling, and A. Fiore, "Spontaneous emission control of single quantum dots by electromechanical tuning of a photonic crystal cavity," Appl. Phys. Lett. **101**, 091106 (2012).
27. Z. K. Bishop, A. P. Foster, B. Royall, C. Bentham, E. Clarke, M. S. Skolnick, and L. R. Wilson, "Electro-mechanical control of an on-chip optical beam splitter containing an embedded quantum emitter," Opt. Lett. **43**, 2142–2145 (2018).
28. S. Abel, F. Eltes, J. E. Ortmann, A. Messner, P. Castera, T. Wagner, D. Urbonas, A. Rosa, A. M. Gutierrez, D. Tulli, P. Ma, B. Baeuerle, A. Josten, W. Heni, D. Caimi, L. Czornomaz, A. A. Demkov, J. Leuthold, P. Sanchis, and J. Fompeyrine, "Large Pockels effect in micro- and nanostructured barium titanate integrated on silicon," Nat. Mater. **18**, 42–47 (2019).
29. A. W. Elshaari, I. E. Zadeh, A. Fognini, M. E. Reimer, D. Dalacu, P. J. Poole, V. Zwiller, and K. D. Jöns, "On-chip single photon filtering and multiplexing in hybrid quantum photonic circuits," Nat. Commun. **8**, 379 (2017).
30. K. Suzuki, G. Cong, K. Tanizawa, S.-H. Kim, K. Ikeda, S. Namiki, and H. Kawashima, "Ultra-high-extinction-ratio 2×2 silicon optical switch with variable splitter," Opt. Express **23**, 9086–9092 (2015).
31. G. Kiršanskė, H. Thyrrestrup, R. S. Daveau, C. L. Dreeßen, T. Pregnolato, L. Midolo, P. Tighineanu, S. Stobbe, R. Schott, A. Ludwig, A. D. Wieck, S. In Park, J. D. Song, A. V. Kuhlmann, I. Söllner, M. C. Löbl, R. J. Warburton, and P. Lodahl, "Indistinguishable and efficient single photons from a quantum dot in a planar nanobeam waveguide," Phys. Rev. B **96**, 165306 (2017).
32. X. Zhou, I. Kulkova, T. Lund-Hansen, S. L. Hansen, P. Lodahl, and L. Midolo, "High-efficiency shallow-etched grating on GaAs membrane for quantum photonic applications," Appl. Phys. Lett. **113**, 251103 (2018).
33. M. B. Ward, O. Z. Karimov, D. C. Unitt, Z. L. Yuan, P. See, D. G. Gevaux, and A. J. Shields, "On-demand single-photon source for 1.3 μm telecom fiber," Appl. Phys. Lett. **86**, 201111 (2005).
34. J. Wu, Y. Liu, B. Zhang, X. Jin, Y. Wang, H. Wang, and X. Yang, "A benchmark test of boson sampling on Tianhe-2 supercomputer," Natl. Sci. Rev. **5**, 715–720 (2018).
35. I. Wilson-Rae, "Intrinsic dissipation in nanomechanical resonators due to phonon tunneling," Phys. Rev. B **77**, 245418 (2008).
36. P. Treutlein, C. Genes, K. Hammerer, M. Poggio, and R. Rabl, *Hybrid Mechanical Systems* (Springer, 2014).
37. F. Lenzini, B. Haylock, J. C. Loredo, R. A. Abrahão, N. A. Zakaria, S. Kasture, I. Sagnes, A. Lemaitre, H.-P. Phan, D. V. Dao, P. Senellart, M. P. Almeida, A. G. White, and M. Lobino, "Active demultiplexing of single photons from a solid-state source," Laser Photon. Rev. **11**, 1600297 (2017).
38. M. Poot and H. X. Tang, "Broadband nanoelectromechanical phase shifting of light on a chip," Appl. Phys. Lett. **104**, 061101 (2014).